Research Article | Vol. 27, No. 24 / 25 November 2019 / Optics Express 34559

Optics EXPRESS

Calibration of systems for quantitative fluorescence analysis of thin layers

PHILIPP HOLZ* AND ALBRECHT BRANDENBURG

Fraunhofer Institute for Physical Measurement Techniques IPM, Heidenhofstraße 8, 79110 Freiburg, Germany

*philipp.holz@ipm.fraunhofer.de

Abstract: Imaging fluorescence analysis is a powerful tool for the characterization of thin functional layers. Due to the development of new components such as cost-efficient and long life diode lasers and LEDs as well as sensitive cameras, the number of industrial in situ sensors based on fluorescence analysis technology increased rapidly in recent years. Of crucial importance for all these new sensors are efficient and robust methods for calibration. Although there are many examples for the calibration of laboratory setups for single specialized applications, there is no standardized method for the traceable device independent calibration of imaging fluorescence systems. This paper presents the evaluation of five different methods for the calibration of systems for quantitative fluorescence analysis. Each method is applied for the calibration of an imaging fluorescence laser scanner. In addition to characterizing the precision of the methods, the work analyzes the usability of the methods for different applications. The results show for the first time that a calibrated IR point sensor can be used for the auto calibration of high resolution imaging inline fluorescence sensors. In addition, we present a novel method for the transfer of calibration data between analysis systems with different optical setups by using a solid material fluorescence standard.

1. Introduction

Measurement systems based on imaging fluorescence analysis are of increasing importance in many industrial applications. These applications range from the determination of surface cleanliness in food processing plants [1] to the detection of oil spills by fluorescence laser scanners installed on airplanes [2]. One promising application is the analysis of the spatial distribution of the thickness of thin lubricant layers in industrial production processes [3,4]. Currently, quantitative measurements of the layer thickness require the individual calibration of each analysis system.

Calibration can be described as a set of procedures that establishes the relationship between measurements on an instrument and the corresponding quantity values realized by standards [5]. Although there are many examples for the calibration of laboratory setups for single specialized applications [6–8], there is no standardized method for the traceable device independent calibration of imaging fluorescence systems. Aim of the work leading to this publication was the development, implementation and evaluation of easy and robust methods for the calibration of fluorescence measurement systems. Each method is characterized regarding its achievable precision as well as its limits. Another focus of the work was to review the usability of the methods for applications in different environments.

In this work, we evaluate five different approaches for the exemplary calibration of a previously presented fluorescence laser scanner [4]. Each method is applied for the calibration of the imaging fluorescence laser scanner.

The most straightforward approach for calibration is the measurement of differently coated samples using a high-resolution balance as reference (**method 1**). As reference tool only an appropriate balance is required. Therefore, theoretically the preparation of gravimetrically

#374311 https://doi.org/10.1364/OE.27.034559
Journal © 2019 Received 2 Aug 2019; revised 31 Oct 2019; accepted 31 Oct 2019; published 11 Nov 2019

Optics EXPRESS

characterized samples is the easiest realizable way for the calibration of fluorescence measurement systems. The biggest advantage of this method is that high-resolution balances are usually calibrated with traceable weighing standards. Thus, the calibration process is directly traceable to official standards. Nevertheless, there are some major limitations in practice. The following three calibration methods overcome these limitations by transferring the traceable gravimetrical calibration to an additional intermediate measurement technology.

Previous publications show that the fluorescence response highly depends both on the lubricant type and the properties of the coated surface [9]. These dependencies require specific calibration work for each layer/substrate combination found in the production process to be monitored. In contrast, systems for infrared absorption measurements (IR sensors) are less sensitive to both the lubricant type and the samples surface. Therefore, we use a gravimetrically characterized IR sensor to indirectly calibrate the fluorescence system on traceable gravimetric standards (**method 2**). This combination e.g. allows the usage of an IR sensor to auto-calibrate a high resolution imaging fluorescence sensor. This would drastically reduce the calibration work.

The precision of commercially available high-resolution balances and IR sensors is not sufficient for the direct determination of the limit of detection of fluorescence sensors. Therefore, we use a previously gravimetrically calibrated multiphase carbon analyzer as reference for the determination of very thin lubricant layers (**method 3**) [9]. An advantages of this analysis technology is the good limit of detection; in addition, there is nearly no dependency on the type of substrate or lubricant. In contrast to the other methods discussed in this paper, all samples are destroyed during the reference measurements of this method.

In all the previously mentioned methods, initially unknown samples are characterized using a traceable measurement technology. Another way to calibrate fluorescence sensors for thin lubricant layers is the preparation of defined lubricant layers. For this work, we use an ink-jet printer for the layer preparation (**method 4**) [4]. For the calibration, varying the number of oil droplets printed per area leads to different area densities. To determine the prepared area densities, the mass of a single droplet is determined. Therefore, the ink jet printer fills a known number of droplets into a flask that is then weighed using an analytical balance.

For all methods described so far, thin layers have to be prepared by suitable coating principles. In addition, all methods described so far use gravimetrical standards as reference. As alternative, we evaluate the use of cuvettes for the easy and fast preparation of lubricant layers (**method 5**). As commonly known, the emission spectra of optically thick layers are shifted towards longer wave length due to reabsorption of short wavelength emission [10]. Therefore, typical proceedings for the acquisition of fluorescence spectra suggest the dilution of optical dense substances to an optical density of 0.1. [10,11]. While most applications of fluorescence measurements use dyes, we examine the auto fluorescence of the lubricants itself. This would require the selection of suitable non-fluorescent solvents for each individual lubricant. To avoid the use of this often hazardous solvents, we developed a custom made thin film cuvette presented in this paper. The cuvette thickness is determined using a 3D confocal microscope as reference.

The use of high-resolution balances and confocal microscopes as reference demands a clean and vibration free work environment to achieve the required accuracy. For better practicability, we suggest to split the calibration process. The sophisticated characterization of the samples can be done in a clean lab environment. In order to transfer the calibration data subsequently, all signals are normalized to a fluorescence intensity standard. For the final on-site calibration in the industrial environment, only the fluorescence signal of the transfer target has to be acquired. We evaluate this new approach as part of method 5. Therefore, we initially analyze lubricant filled thin-film cuvettes with a fluorescence spectrometer. The results gathered with the spectrometer are then transferred to an imaging fluorescence laser scanner.

As described by Resch-Genger et al., there are different levels of increasing sophistication in methods for characterizing the performance of fluorescence sensors. The first level is the

Optics EXPRESS

day-to-day characterization of the performance of an individual system. The second level is the comparison of instruments build to the same or a directly comparable specification. The third and most difficult level is the comparison of instruments of different manufactures built to different specifications. [12] The method developed for the transfer of calibration data therefore can easily be adopted for the quick comparison of different fluorescence sensors.

2. Theory on quantification of thin-film fluorescence

The following section describes the physical fundamentals required to quantify the thickness of thin fluorescent layers based on the fluorescence signal.

2.1. Absorption of excitation light

According to Beer–Lambert law, incident light with the power P_0 is attenuated proportional to the optical path length l of an absorbing layer and the attenuation coefficient α of the medium at the wavelength of the incident light. Therefore, the transmitted power P_1 after the light travelled the path length l is described by

$$P_1(l) = P_0 \exp(-\alpha l). \tag{1}$$

The power of the absorbed light P_{abs} over a certain optical path length l is described by

$$P_{\text{abs}}(l) = P_0(1 - \exp(-\alpha l)). \tag{2}$$

In general, for low absorbance values $\alpha l \ll 1$ the first term of the Taylor series can be used as valid approximation for the exponential term in Eq. (2)

$$\exp(-\alpha l) \approx 1 - \alpha l. \tag{3}$$

Application of Eq. (3) on Eq. (2) leads to

$$P_{\text{abs}}(l) = P_0 \alpha l. \tag{4}$$

As visualized in Fig. 1, for the developed thin film cuvette as well as for thin layers in general, different excitation angles lead to different absorption path lengths l.

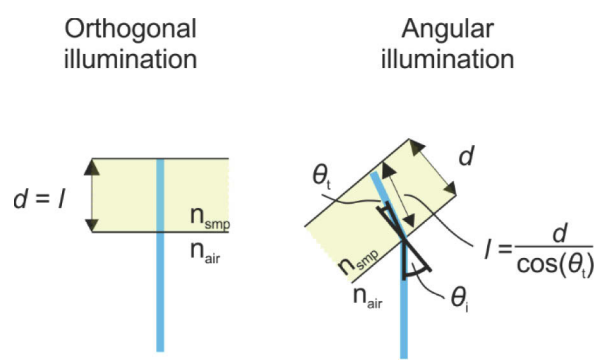

Fig. 1. Light path for orthogonal and angular illumination of an absorptive layer.

It is commonly known that the change of the direction of light due to refraction can be described using Snell's law [13]. Refraction at the interface between air and a sample with refractive index n_{smp} is described as

$$n_{\text{air}} \sin\theta_{\text{i}} = n_{\text{smp}} \sin\theta_{\text{t}}, \tag{5}$$

with the angle of incident θ_{i} and the angle θ_{t} of the transmitted light beam. For a constant cuvette thickness d, the optical path length l increases with increasing angle. This geometrical relation is

Optics EXPRESS

inversely proportional to the cosine function

$$\cos\theta_{\mathrm{t}} = \frac{d}{l}. \tag{6}$$

Using Eq. (5) leads to the following relation

$$l(\theta_i,\ d) = \frac{d}{\cos(\arcsin({}^{n_{\mathrm{air}}}/_{n_{\mathrm{smp}}}\sin\theta_{\mathrm{i}}))}. \tag{7}$$

2.2. Emission of fluorescence light

The ratio of the number of emitted photons to the number of absorbed photons is defined as quantum yield ϕ. The steady-state fluorescence intensity per absorbed photon can be expressed as a function of the wavelength of the emitted photons F_λ (λ_{em}) in nm^{-1}

$$\int_0^\infty F_\lambda(\lambda_{\mathrm{em}})d\lambda = \phi. \tag{8}$$

F_λ (λ_{em}) represents the fluorescence spectrum. In practice, the steady-state fluorescence intensity P_{f} (λ_{em}) measured at wavelength λ_{em} is proportional to F_λ (λ_{em}) and to the number of photons absorbed at the excitation wave length λ_{ex} [14]. Using Eq. (4), the fluorescence emission for low absorbance values αl can thus be written as

$$P_f(l, \lambda_{\mathrm{em}}) = P_0\alpha l F_\lambda(\lambda_{\mathrm{em}}). \tag{9}$$

Considering Eq. (7), the angle of illumination θ_{i} has to be considered to determine the layer thickness d, leading to

$$P_f(d, \lambda_{\mathrm{em}}, \theta_{\mathrm{i}}) = P_0\alpha l(\theta_{\mathrm{i}},\ d)F_\lambda(\lambda_{\mathrm{em}}). \tag{10}$$

In practice, the detector signal U_{d} is determined by the spectral response S_{d} (λ_{em}) of the detector including detector optics. In addition, a so-called geometry factor is introduced to describe the portion of the fluorescence light reaching the detector. In literature, this geometry factor typically describes the ratio of the solid angle of fluorescence emission, the solid angle of detection and the size of the illuminated volume. Therefore, this factor depends on both the instrument and the sample [15,16]. In this work, we split the geometry factor. The proportionality factor G_{in} (θ_{det}) describes the aperture of the instrument. The proportionality factor G_{sa} (θ_{det}) describes the angular emission characteristics of the sample. Both factors vary as function of the observation angle θ_{det}. By application of these factors on Eq. (10), the detector signal U_{d} is described by

$$U_{\mathrm{d}}(d, \lambda_{\mathrm{em}}, \theta_{\mathrm{i}}, \theta_{\mathrm{det}}) = G_{\mathrm{in}}(\theta_{\mathrm{det}})G_{\mathrm{sa}}(\theta_{\mathrm{det}})S_{\mathrm{d}}(\lambda_{\mathrm{em}})P_{\mathrm{f}}(d, \lambda_{\mathrm{em}}, \theta_{\mathrm{i}}). \tag{11}$$

Finally, the total power $U_{\mathrm{d},\Delta\lambda}$ detected by a fluorescence sensor is defined by the cut-off wavelengths λ_{l} and λ_{h} of the edge-pass filters for the suppression of excitation and ambient light. Using Eq. (11) leads to

$$U_{\mathrm{d},\Delta\lambda}(d, \theta_{\mathrm{i}}, \theta_{\mathrm{det}}) = G_{\mathrm{in}}(\theta_{\mathrm{det}})G_{\mathrm{sa}}(\theta_{\mathrm{det}})P_0\alpha l(\theta_{\mathrm{i}},\ d)\int_{\lambda_{\mathrm{l}}}^{\lambda_{\mathrm{h}}} F_\lambda(\lambda_{\mathrm{em}})S_{\mathrm{d}}(\lambda_{\mathrm{em}})d\lambda. \tag{12}$$

For many fluorescence sensors, the spectral response S_{d} (λ_{em}) of the detector can be assumed as constant for light in the wavelength range from λ_{l} to λ_{h}. Fluorescence spectrometers often offer the possibility for an automated correction of the spectral dependency S_{d} (λ_{em}). In these cases Eq. (12) can be simplified to

$$U'_{\mathrm{d},\Delta\lambda}(d, \theta_{\mathrm{i}}, \theta_{\mathrm{det}}) = S_{\mathrm{d}}G_{\mathrm{in}}(\theta_{\mathrm{det}})G_{\mathrm{sa}}(\theta_{\mathrm{det}})P_0\alpha l(\theta_{\mathrm{i}},\ d)\int_{\lambda_{\mathrm{l}}}^{\lambda_{\mathrm{h}}} F_\lambda(\lambda_{\mathrm{em}})d\lambda. \tag{13}$$

Optics EXPRESS

2.3. Calibration of fluorescence sensors

In practice, we usually calibrate fluorescence sensors with a fixed power P_0 of the excitation light, constant angles θ_i and θ_det as well fixed cut-off wavelengths λ_l and λ_h. Since normally each calibration is only valid for a specific substance, the absorption coefficient α and the fluorescence spectrum F_λ are constant, too. Therefore, Eq. (12) can be simplified to

$$U'_{d,\Delta\lambda}(d) = kd, \tag{14}$$

with the proportionality coefficient k describing the relation between the layer thickness d and the detector signal $U'_{d,\Delta\lambda}$. This proportionality coefficient k is specific for each combination of fluorescence sensor and fluorescent substance.

For the actual calibration, we analyze the fluorescence emission of samples coated with different lubricant layers. Subsequently, we determine the proportionality coefficient k by calculating the best linear fit function between the layer thickness d determined by a reference method and the detector signal $U'_{d,\Delta\lambda}$ acquired with the fluorescence sensor. For the comparison of the different calibration methods, we evaluate the mean deviation of the samples used for calibration from the linear fit function.

2.4. Normalized fluorescence response

As mentioned in the introduction, we suggest the transfer of fluorescence calibration data by normalizing all signals to the signal emitted by a fluorescence intensity standard. To determine this normalized fluorescence response F_n, we calculate the quotient of the detector signal $U_\mathrm{d,\ sa}$ of the sample and the signal $U_\mathrm{d,\ st}$ detected when analyzing a fluorescent reference target. Due to this normalization the power P_0 of the excitation source and the instrument-specific proportionality factor G_in (θ_det) are mathematically canceled. This leads to the system-independent normalized fluorescence response F_n described by

$$F_n\,(d, \lambda_\mathrm{em}, \theta_\mathrm{i}, \theta_\mathrm{det}) = {U_\mathrm{d,sa}}/{U_\mathrm{d,st}} \tag{15}$$

Therefore, the normalized fluorescence response F_n describes the emission of fluorescent layers as a function of the layer thickness d, the detection wavelength λ_em and the angles of illumination θ_i as well as observation θ_det.

As described by Eq. (7), the optical path length inside the absorptive layer depends on the angle of illumination θ_i and the refractive index of the absorptive layer n_smp. If sample and transfer target show similar indices of refraction, this angle dependency is mathematically canceled as well. In this case, the normalized fluorescence response is independent of the illumination angle θ_i.

In this work, we only compare fluorescence sensors with identical excitation wavelengths. Since the attenuation coefficient α varies as function of the excitation wavelength, in general the normalized fluorescence response F_n is a function of the excitation wavelength as well.

3. Material and methods

3.1. Optical setups

In this work we exemplarily calibrate a previously described fluorescence laser scanner [4]. This custom developed system uses scanning mirrors in combination with laser induced fluorescence in order to monitor the spatial distribution of thin fluorescent layers. For one of the presented calibration methods we use the data acquired with a fluorescence spectrometer. Figure 2 presents the schematics of the optical setups of both systems.

Optics EXPRESS

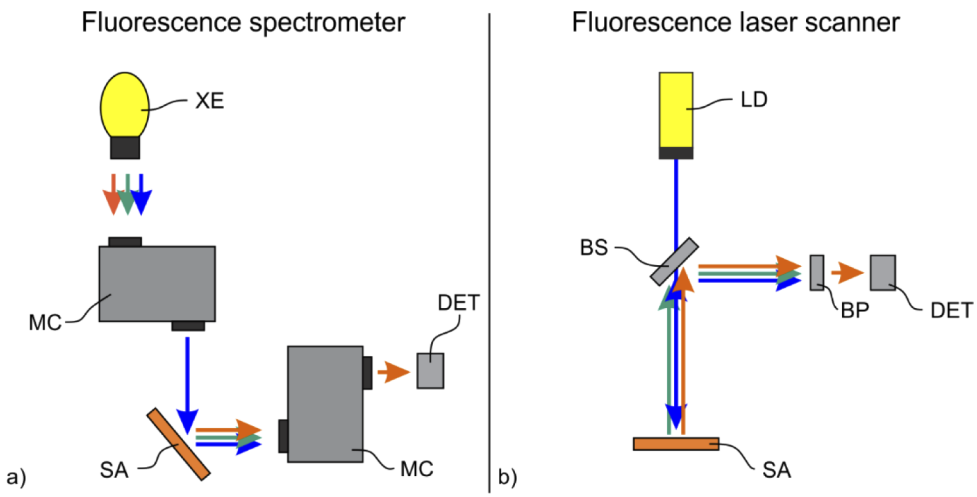

Fig. 2. Schematics of the optical setups of the spectrometer (a) and of the fluorescence laser scanner (b) used in this work. In the spectrometer the light of a Xenon Lamp (XE) illumintes the sample (SA). Both the excitation and the detection wavelength can be adjusted by two monochromators (MC). The fluorescence laser scanner uses a laser diode (LD) for illumination of the sample. The combination of a beam splitter (BS) and a band pass filter (BP) determine the wavelengths directed to the detector (DET).

3.1.1. Fluorescence laser scanner

The fluorescence laser scanner uses a 405 nm diode laser module with 300 mW optical power for the excitation of the samples. The light of the laser is focused on the bottom of the sample chamber. During the scan, the excitation laser induces fluorescence locally on the probe inside the sample chamber. For simplification, the scanning mirrors are not shown in the schematic of the fluorescence laser scanner in Fig. 2(b). The fluorescence light is emitted into the sample chamber and a certain portion of this emission is collected back by the scanning mirrors. A chromatic beam splitter is used to deflect fluorescence light in a wavelength range from $\lambda_l = 420$ nm to $\lambda_h = 500$ nm on the detector. In practice, the properties of the previously listed components are described by the system-specific proportionality factor G_{in} (θ_{det}) introduced with Eq. (11). For the detection of the fluorescence signals, we use a photomultiplier module. According to the datasheet of the photomultiplier, the spectral response S_d can be assumed as constant in the wavelength range used in this fluorescence laser scanner.

The optical system is installed 330 mm above the bottom of the sample chamber. The size of the largest samples analyzed in this work is 70×70 mm^2. Therefore, the maximum required deflection of the laser beam is $\pm 6°$. For simplification, we assume identical angles of $\theta_i = \theta_{det} = 0°$ both for illumination and as observation. The filter glass of the housing prevents the excitation laser from leaving the sample chamber, thus ensuring laser safety.

After each measurement, the fluorescence laser scanner saves a 2D image of the acquired fluorescence signals. Therefore, each pixel of the image contains a 16 bit floating point value of the detector voltage. The optical resolution of the laser scanner is better than 0.5 mm.

3.1.2. Fluorescence spectrometer

To obtain the fluorescence spectrum F_λ (λ_{em}) we use a bench top fluorescence spectrometer (Jasco, FP-5800). This spectrometer uses a Xenon lamp for the excitation of the fluorescent samples. The excitation wavelength is selected using a monochromator. In the experiments leading to the results presented in this paper we set the excitation wavelength to $\lambda_{ex} = 405$ nm at a bandwidth of

Optics EXPRESS

5 nm. A second monochromator is used for the acquisition of the spectrum of the fluorescence emission. In the presented experiments we acquired the fluorescence spectrum in the wavelength range from $\lambda_l = 415$ nm to $\lambda_h = 700$ nm. To prevent direct reflexes the sample is illuminated at an angel of $\theta_i = 50°$ leading to an angle of observation of $\theta_{det} = 40°$. For simplification, we assume identical angles $\theta_i = \theta_{det} = 45°$ both for illumination and as observation.

Before the acquisition of the spectra for this work, the spectral characteristics of the spectrometer was corrected. As suggested by Jasco, the spectral correction of the detector was performed using a calibrated light source and the spectral properties of the Xe lamp were determined using a Rhodamine B ethylene glycol solution as standard. Therefore, the spectral response S_d can be assumed as constant. The spectrometer software exports all spectra information in radiometric quantities.

3.2. Calibration method 1: analysis of gravimetrically characterized samples

The most straightforward approach for calibration is the measurement of differently coated samples. For this calibration method, we prepare lubricant layers with an initially unknown thickness. Subsequently, we determine the average layer thickness d of the prepared layer with a high-resolution balance. Since the prepared lubricant layer will never be perfectly homogeneous, we use the area density ρ_A of lubricant applied to the surface for the description of the prepared samples. This area density ρ_A is calculated by

$$\varphi_A = \frac{m_1 - m_0}{A}, \tag{16}$$

with A describing the sample's surface, m_0 describing the weight before coating and m_1 describing the weight after coating.

The then known samples are subsequently analyzed with the laser scanner. As described in Eq. (15), we normalize the detector signal in each pixel on the signal of the reference target to obtain the normalized fluorescence response F_n. In this work, we use a solid disc made of Spectralon fluorescence material (Labsphere Type 461: USFS-461-020) as reference target. According to Labsphere, the fluoropolymer material Spectralon is used as a matrix for inorganic fluorophores which are photochemically stable compared to their organic counterparts [17]. Due to the spatial inhomogeneity of the samples, we calculate the average fluorescence response of all pixels covering the samples surface.

3.2.1. Sample preparation

For sample preparation, metal sheets of the size of 70×70 mm^2 are cut out of aluminum silicate coated steel (Thyssen Krupp) with a very smooth surface as well as hot-dip galvanized electric discharged textured (EDT) steel (Voest). Before the coating with oil all samples are cleaned using Heptane. For the work presented, we applied the forming oil KTL N 16 as well as the lubricants for corrosion protections RP 4107 S and RP 4107 LV.

In literature, different methods for the preparation of thin lubricant layers are suggested. In previous work we used a spray unit for the preparation of the layers [9]. One drawback of this method is that depending on the surface energy, droplets applied on the surface do not form a homogeneous film, as required for the experiment. Another possible coating technique is dip-coating [18]. Whereas most applications require the imaging fluorescence analysis on just one sample face, with dip-coating lubricant is applied on both the bottom as well as the front surface.

To overcome these drawbacks, we use a rubber wallpaper roll for the application of the lubricant layers in this work. To prevent the absorption of lubricant by the rubber, we cover rubber roll with aluminum foil. For the actual coating, first about one milliliter of the lubricant is applied on a clean plane aluminum foil. Subsequently, the lubricant is homogeneously distributed on the

Optics EXPRESS

foil using the rubber roll. To adjust the thickness of the final coating, we vary the area lubricated on the aluminum foil. After the distribution of the lubricant on the aluminum foil, the oily roll is used for the coating of the actual metal samples.

The weight of all metal samples is determined before and after coating using a high-resolution balance (Sartorius, MSE225P-100-DU). The average area density of the lubricant layer is then calculated according to Eq. (16). Figure 3 exemplarily shows fluorescence images acquired with the fluorescence laser scanner of samples with different amount of lubricant applied on the surface.

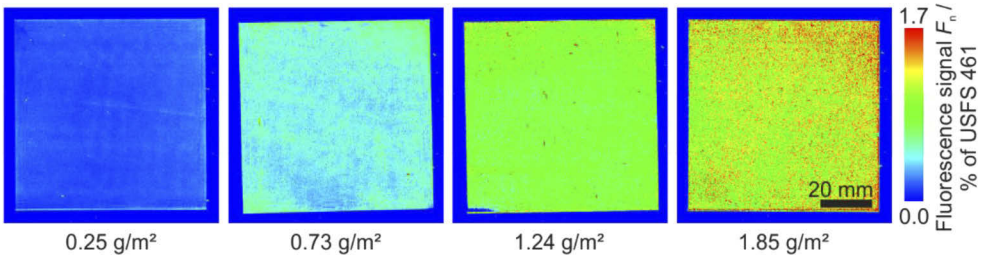

Fig. 3. Fluorescence images of different layers of the lubricant KTL N 16 applied on EDT textured steel. All lubricant layers have been applied with an aluminum covered wallpaper roll. The fluorescence images were acquired with the fluorescence laser scanner.

3.3. Calibration method 2: infrared absorption measurements as reference

In this calibration method, the results of an alternative optical measurement technology are used as reference. The most common technology for the measurement of lubricant layers in the range of 0.5 to 5 g/m^2 is the use of infrared absorption sensors. In contrast to fluorescence measurements, infrared-absorption measurements are less sensitive to variations of both the lubricant type and the samples surface.

3.3.1. Sample preparation

For this method, the samples are coated in the same way as for method 1. For the work presented in this paper, we use the same lubricant and metal samples as described in method 1.

In contrast to method 1, we characterize the samples with the infrared absorption sensor NG2 provided by Infralytic GmbH. It is commonly known that lubricants based on mineral oils show a strong absorbance in the range of 3000 to 2800 cm^{-1} due to the stretching vibrations of their C-H bonds [19,20]. In contrast, the lubricant layer does not absorb infrared light outside this range. To distinguish between signal losses due to scattering and the absorbance caused by the lubricant layer the NG2 system normalizes the signals at the absorbance wavelength around 2900 cm^{-1} to the signal at reference wavelengths on both sides of the peak. Infralytic GmbH calibrated the NG2 sensor in advance to the experiments. In general, the NG2 sensor allows the calibration for different surfaces as well for different lubricant types. In this work, these functions have not been activated to allow the comparison of the raw data of both the fluorescence analysis and the infrared absorption measurement. Therefore, the results of the infrared absorption measurements were acquired using the so-called 'TEST' channel of the NG2 sensor.

The NG2 sensor uses a halogen lamp optimized for the mid-IR spectrum to illuminate the sample surface. A dark field illumination is used to minimize the influence of the light reflected directly from the lubricant layer surface. In each measurement, the NG2 sensor measures the average lubricant density within a spot with a diameter of 8 mm. Since the prepared lubricant layer will never be perfectly homogeneous, we used two linear stages to scan the complete surface of the sample with the infrared absorption sensor. To avoid errors, a distance of approx. 5 mm is

Optics EXPRESS

kept from the samples edge while scanning. The stages are moved in steps of 5 mm between the sampling of two values. Figure 4 exemplarily shows the comparison of the results of the analysis of the same sample with the fluorescence laser scanner (a) and the IR sensor NG2 (c).

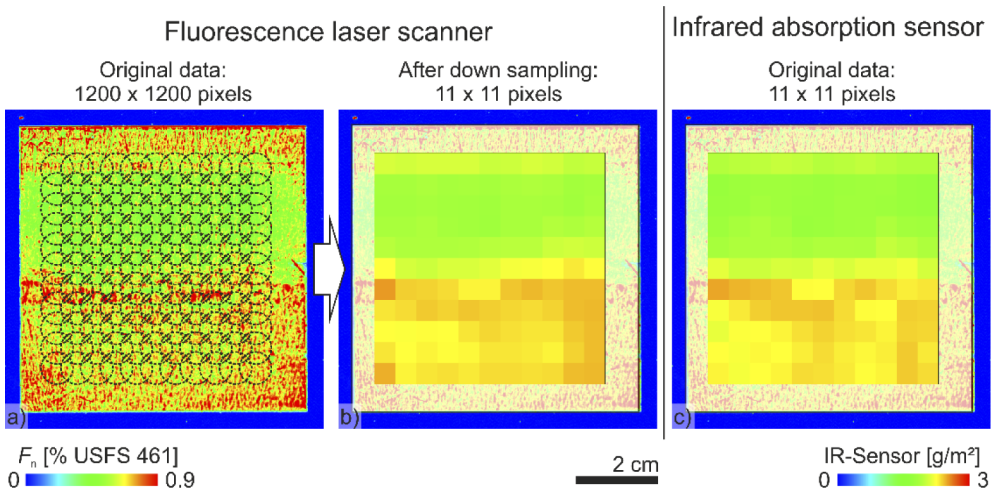

Fig. 4. Comparison of false color images showing the analysis results of the same sample with the fluorescence laser scanner (a&b) and the IR sensor NG2 (c). For this experiment, an EDT structured steel sample was coated with an average area density of 1.25 g/m^2 of the lubricant RP 4107 S.

As shown in Fig. 4, the images acquired with the fluorescence laser scanner initially consist of 1200×1200 pixels, whereas we analyzed 121 positions with the calibrated IR sensor. We calculated the average fluorescence signal at each of the 121 positions to exemplarily compare the results of both measurement technologies in Fig. 4. The dashed circles in Fig. 4(a) visualize the measurement positions of the IR sensor. Figure 4(b) shows the result for the down sampled fluorescence image. To minimize errors, in the following measurements we used the average of all values detected on the sample surface by both sensors for the calibration.

3.4. Calibration method 3: multiphase carbon analyzer measurements as reference

In this calibration method, the results of multiphase carbon analyzer measurements are used as reference. In contrast to the previously presented technologies for reference measurements, this method destroys the samples during the reference measurement. Therefore, we acquire fluorescence images of the samples directly after the preparation. For the calibration of the fluorescence sensor, we correlate the amount of surface carbon with the average fluorescence signal.

3.4.1. Sample preparation

For the work presented in this paper, we prepared thin layers of a rolling oil on clean copper foils. The samples are coated in the same way as for method 1. For the reference measurement, we cut the samples into small slices of the size of 1×2 cm^2. The multiphase carbon analyzer (LECO Corporation, RC612) combusts the lubricant on the samples surface at temperatures up to 750° C [21]. Since the samples are combusted in a pure oxygen stream, carbon released by the lubricant reacts to carbon dioxide. A calibrated infrared detector analyzes the total amount of carbon dioxide. It has to be considered that the result of the multiphase carbon analysis includes carbon combusted on both sides of the sample surface. Since the fluorescence laser scanner

Optics EXPRESS

does not analyze the bottom side of the samples, this sample face has to be free of any organic contamination.

3.5. Calibration method 4: printing of defined lubricant layers

In the previously presented methods, initially unknown samples are characterized using a traceable measurement technology. In contrast, in this method defined lubricant layers are prepared with an ink-jet printer (Fujifilm, Dimatix 2831).

For the calibration, different area densities are achieved by varying the number N of oil droplets printed per area A. Considering the weight m_d of a single lubricant droplet, the printed area density ρ_A is described by

$$\rho_A = \frac{N}{A} m_\mathrm{d}. \tag{17}$$

For the calibration of the fluorescence sensor, we correlate the printed area density with the average fluorescence signal.

3.5.1. Sample preparation

For the work presented in this paper, we printed layers of the certified reference material BAM-K009 on a sandblasted aluminum sample. BAM-K009 is a lubricant oil based on the additive free lubricant oil HVI 50 provided by Shell Global Solutions GmbH. Homogeneity and stability of the mass fraction of the boiling range C10 - C40 are certified by BAM Federal Institute for Materials Research and Testing [22].

To determine the average weight m_d of a single lubricant droplet we determined the weight of the aluminum sample before and after printing using an analytical balance (Sartorius, CP225D). The weight of all 486 000 droplets dispensed while printing was determined to 6.22 ± 0.1 mg. Therefore, the average mass of a single lubricant droplet is $m_\mathrm{d} = 1.27 \pm 0.02$ ng.

The number of droplets N varies in the range of 18 000 to 90 000 for the results shown in this paper. Since the printed area is $A = 15 \times 15$ mm^2, this leads to lubricant densities in the range of $\rho_\mathrm{A} = 51.2 \pm 0.8$ µg/cm^2 to $\rho_\mathrm{A} = 10.2 \pm 0.2$ µg/cm^2.

3.6. Calibration method 5: Use of thin film cuvettes and device independent transfer of spectrometer measurements using a reference target

All methods described so far use gravimetrical standards as reference. As alternative, we evaluate the use of a custom designed thin film cuvette for the easy and fast preparation of lubricant layers. Different spacers inside the cuvette lead to different film thickness. For the determination of the thickness of the cuvette, we use a 3D confocal laser scanning microscope (Keyence, VK 9700).

As described in the introduction, we use this experiment to analyze the possibility of transferring calibration data between different fluorescence sensors. Therefore, we compare the normalized fluorescence response $F_{\mathrm{n,\ sp}}$ measured with a fluorescence spectrometer with the normalized fluorescence response $F_{\mathrm{n,\ ls}}$ detected with the fluorescence laser scanner. As described by Eq. (15), the normalized fluorescence response is a function of the layer thickness d, the detection wavelength λ_em and the angles of illumination θ_i as well as observation θ_det. For the conversion of the normalized fluorescence response between both optical systems, we have to consider differences in the parameters describing the instrument specification. Table 1 compares these instrument specific parameter for both optical systems.

To consider these different optical setups, we introduce a series of correction factors C_x. Therefore, the normalized fluorescence response $F_{\mathrm{n,\ ls}}$ of the laser scanner can be described as a

Optics EXPRESS

Table 1. Comparison of the instrument specific parameter of the optical systems used in the presented work.

	Fluorescence spectrometer	Fluorescence laser scanner
Excitation wavelength λ_{ex}	405 nm	405 nm
Detector bandwidth λ_l to λ_h	415 to 700 nm	420 to 500 nm
Illumination angle θ_i	45°	0°
Observation angle θ_{det}	45°	0°

function of the normalized fluorescence response $F_{n,\,sp}$ gathered with the spectrometer by

$$F_{n,\,ls}(d) = F_{n,\,sp}(d) \prod C_x. \tag{18}$$

The first difference between both systems is defined by the cut-off wavelengths λ_l and λ_h of the detector. For the correction of this difference, we introduce the correction factor C_s as

$$C_S = \int_{420\text{nm}}^{500\text{nm}} F_\lambda(\lambda_{em})d\lambda \Big/ \int_{415\text{nm}}^{700\text{nm}} F_\lambda(\lambda_{em})d\lambda. \tag{19}$$

This correction has to be applied on both the fluorescence spectrum of the reference target as well as the emission of the sample. Therefore, we introduce the spectral correction $C_{s,\,ref}$ for the reference target and the spectral correction $C_{s,\,smo}$ for the sample.

Furthermore, both systems have different angles of illumination θ_{ex}. As described by Eq. (7), the illumination angle influences the optical path length $l(\theta_{ex})$ for liquid layers. To consider this difference, we introduce the factor C_{ex}. This factor is defined as

$$C_{ex} = {l(\theta_{ex,\,ls})}/{l(\theta_{ex,\,sp})}. \tag{20}$$

Since we use a solid material transfer target, only a correction factor $C_{ex,\,smp}$ for the liquid sample is required.

Thirdly, the angles of observation θ_{det} differ between both systems. Therefore, the angular emission characteristics of the sample respectively transfer target have to be considered by introducing the correction factor C_{det} described by

$$C_{det} = {G_{sa}(\theta_{det,\,ls})}/{G_{sa}(\theta_{det,\,sp})}. \tag{21}$$

This correction has to be applied on both the fluorescence spectrum of the reference target as well as the emission of the sample. Therefore, we introduce the correction factor $C_{det,\,ref}$ for the reference target and the correction factor $C_{det,\,smp}$ for the sample.

Combining Eqs. (19) to (21) leads to

$$F_{n,\,ls}(d) = F_{n,\,sp}(d) \frac{C_{ex,\,smp} C_{s,\,smp} C_{det,\,smp}}{C_{s,\,ref} C_{det,\,ref}}. \tag{22}$$

For clarity in the following sections, we summarize all correction factors describing angular dependencies to the factor C_θ defined as

$$C_\theta = \frac{C_{ex,\,smp} C_{det,\,smp}}{C_{det,\,ref}}. \tag{23}$$

3.6.1. Sample preparation

As discussed in the introduction, we use a thin film cuvette for the characterization of the lubricants in the spectrometer. Based on the oil type and excitation wavelength, film thicknesses

Optics EXPRESS

in the range from 20 to 100 µm are required to achieve the desired optical densities of less than 0.1. Thin film liquid cells for transmission measurements are commercially available. These liquid cells use spacers to realize different thicknesses. Due to their bulky design and the use of fluorescent materials, all cuvettes known to the authors are unsuitable for the fluorescence measurements presented in this work. In literature, there are examples for the use of different shims for the calibration of fluorescence sensors [3], but the presented setup is not compatible to standard fluorescence spectrometers. Therefore, we developed a new custom-made cuvette. As shown in previous experiments, the fluorescence signal depends on both the fluorescent layer as well as the substrate properties [9]. Thus, the cuvette allows the preparation of thin layers on top of different substrates ranging from transparent glass slides to textured metal sheets. Figure 5 shows the final cuvette design. The cuvette's dimensions are $38 \times 64 \times 15$ mm^3.

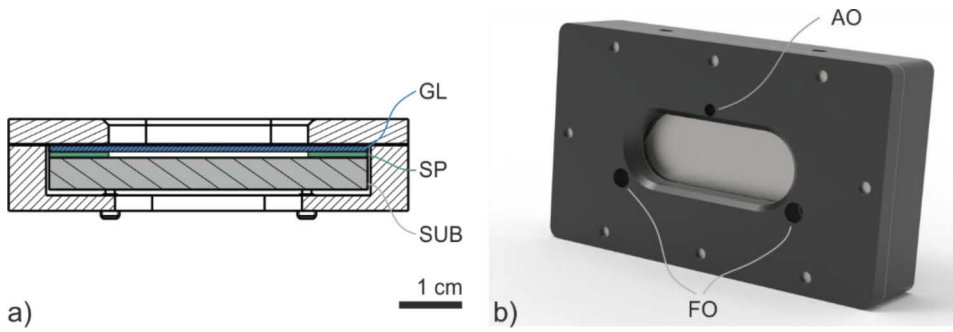

Fig. 5. Profile drawing (a) and sketch (b) of the custom-made thin film cuvette used in this work. To adjust the film thickness, different spacers (SP) are placed between the substrate (SUB) and the cover glass (GL). The cuvette is filled through two sealable filling holes (FO). A third opening acts as air outlet (AO).

The cuvette's body is made of a black anodized aluminum frame. Different spacers allow the implantation of different film thickness. The spacers are laser cut out of aluminum foil. For the work presented in this paper, we use aluminum foils with thickness of 10, 30 and 50 µm. The spacers are inserted between a cover glass and the substrate. To allow the use of substrate materials with different thicknesses, the substrate is pressed towards the spacer and cover glass using screws. For the work presented, we use glass slides as substrate. Due to the potential unevenness of both the spacer and the substrate material, the thickness of the sample chamber may vary with each assembly of the cuvette. Therefore, we use a 3D confocal laser scanning microscope (Keyence, VK 9700) to measure the actual thickness of the cuvette after each assembly. After the measurement of the cuvette's thickness, the cuvette is filled using a pipette. The designed cuvette is filled through two holes. A third hole allows the emission of air to prevent air bubbles inside the cuvette's volume. To prevent evaporation of volatile substances, the cuvette can be shut by three headless screws.

As previously described by Eq. (23), knowledge of the angular dependency of the fluorescence emission of both the thin film cuvette as well as reference target is required for the transfer of the normalized fluorescence response F_n between different optical setups. Figure 6 shows sketches of setups used to analyze these angular dependencies. Figure 6(a) shows the setup for the analysis of the angular emission characteristics G_sa (θ_det) of the sample. For the analysis, we place the samples orthogonal in the light path of a 405 nm laser diode. For the angular resolved detection of the fluorescence emission, we mount a detector optics on a rotatable arm. For this experiment, we used the same detector optics as used in the laser scanner, consisting of an imaging lens, a band pass filter and a photomultiplier tube.

Optics EXPRESS

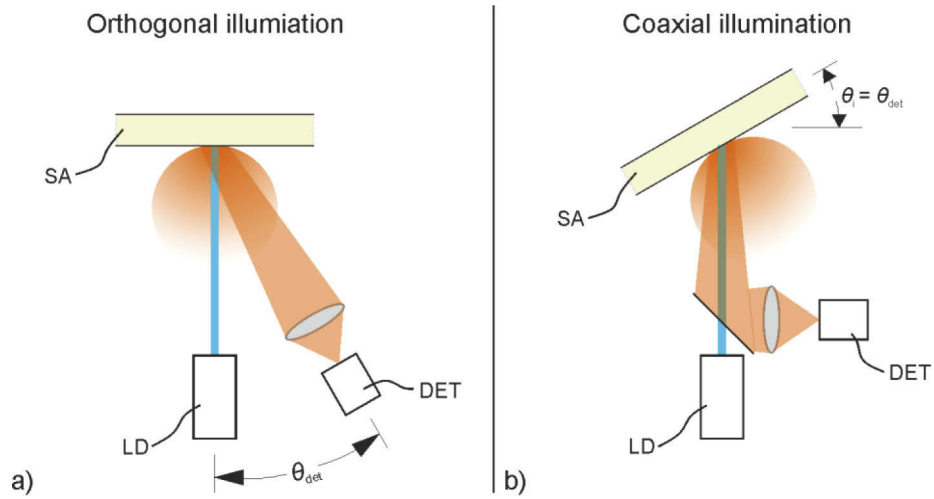

Fig. 6. Setups used for the analysis of the angular dependency of the fluorescence emission of the thin film cuvette as well as the transfer target. The first setup (a) allows the analysis of the angular emission characteristics G_{sa} (θ_{det}). The second setup allows the characterization of the angular dependency C_θ for coaxial systems. In both setups, the sample (SA) is illuminated with a laser diode (LD) with light at 405 nm wavelength. The fluorescence emission is analyzed using a detector module (DET) consisting of a bandpass filter and a photomultiplier tube. Excitation light is visualized in blue color, whereas the fluorescence emission is visualized in orange color.

According to Table 1, both systems used in this work can be assumed as coaxial setups. Figure 6(b) shows the setup for the analysis of the emission characteristics at coaxial illumination. Therefore, we use the setup presented in Fig. 6(b) to determine the angular dependency C_θ. For this experiment, we placed the thin film cuvette as well as reference target on a goniometer stage inside the sample chamber of the fluorescence laser scanner used in this work. For the analysis of the angular dependency of the fluorescence emission, the average signal of the sample is evaluated in the acquired fluorescence images.

4. Results and discussion

4.1. Calibration method 1: analysis of gravimetrically characterized samples

Figure 7 shows results for the calibration of the fluorescence laser scanner by the measurement of differently coated samples. All lubricant layers were gravimetrically characterized using a high-resolution balance as reference. As described by Eq. (15), we normalize all fluorescence signals to the fluorescence signal detected while measuring the fluorescence standard USFS-461.

The results presented in Fig. 7 clearly show an increase of the fluorescence signal as linear function of the layer thickness, as expected by Eq. (14). Figure 7(a) shows the calibration for the lubricants for corrosion protection RP 4107 S and RP 4107 LV applied on EDT textured steel blanks. Figure 7(b) shows the calibration for the application of layers of the forming oil KTL N 16 on both EDT textured and smooth aluminum silicate coated steel blanks. The difference between the calibration results for both oils for corrosion protection is less than 15%. In contrast, we see a difference of one order of magnitude between the fluorescence signals per layer thickness emitted by the forming oil KTL N 16 and the fluorescence response of the lubricants for corrosion protection.

Optics EXPRESS

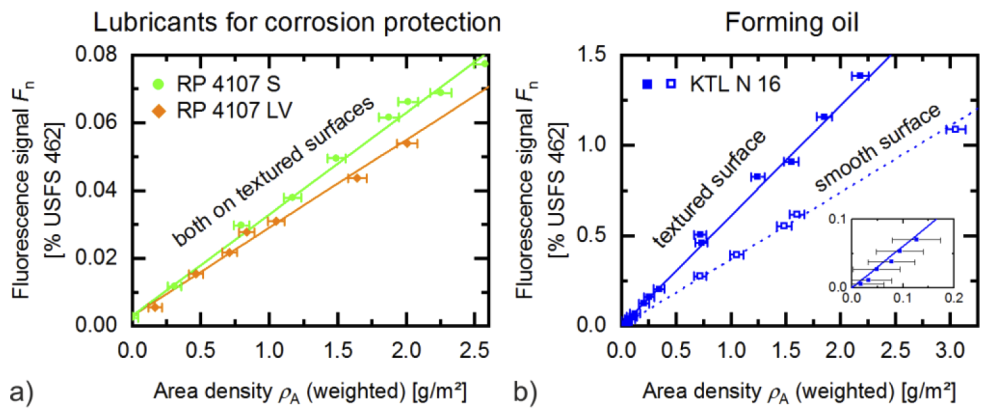

Fig. 7. Calibration of a fluorescence laser scanner for three different oil types. For the calibration, the lubricant layers were gravimetrically characterized using a high resolution balance as reference. The left plot (a) shows the calibration for two lubricants for corrosion protection applied on EDT textured steel blanks. The right plot (b) compares the calibration results for the forming oil KTL N 16 applied on both EDT textured and smooth aluminum silicate coated samples

Figure 7(b) shows the comparison of the calibrations for the same lubricant KTL N 16 on different steel substrates. The different slopes between both calibration curves can be explained by different reflectivity and scatter properties of the metal substrates.

The linear relations between the fluorescence signal F_n and the gravimetrically determined area density ρ_A are visualized as continuous lines in Fig. 7. The average deviations between the linear fit function and the sample measurements are $\Delta\rho_{A,\emptyset} = \pm 0.03$ g/m^2 for KTL N 16, $\Delta\rho_{A,\emptyset} = \pm 0.05$ g/m^2 for RP 4107 LV, and $\Delta\rho_{A,\emptyset} = \pm 0.06$ g/m^2 for RP 4107 S applied on EDT textured steel surfaces. The average relative deviation between the linear fit function and the sample measurements for all samples with area densities over 0.2 g/m^2 is $\Delta\rho_{A,\emptyset} = \pm 5\%$.

The uncertainty of the weighing was determined by multiple measurements of a clean sample. Based on this experiment, we assume an uncertainty of $\Delta m = \pm 0.1$ mg for weighing. The samples used in this work had a lateral length of (70 ± 0.5) mm. Therefore, the area of the samples is A=(49 ± 0.7) cm^2. For the calculation of the error bars in Fig. 7 and Fig. 8, we apply the propagation of uncertainty on Eq. (16). Therefore, the uncertainty $\Delta\rho_A$ for the determination of the area density by weighing is described by

$$\Delta\rho_A = \frac{\Delta m_1}{A} + \frac{\Delta m_0}{A} + \frac{m_1 - m_0}{A^2}\Delta A \tag{24}$$

Considering Eqs. (16) and (24), the application of e.g. $m_1 = (4.5 \pm 0.1)$ g/m^2 of lubricant creates a layer with an average area density of $\rho_A = (0.9 \pm 0.06)$ g/m^2. The constant uncertainty caused by the weighing leads to an increase of the relative error with decreasing layer thicknesses. For area densities lower than 0.2 g/m^2 the relative error induced by the reference method is larger than $\pm$ 20%. Therefore, we suggest the use of this calibration method for lubricant layers with area densities down to 0.2 g/m^2.

It has to be considered, that our assumption for the uncertainty Δm is one order of magnitude higher, as predicted by the calibration certificate of the balance. Therefore, the uncertainty can be reduced, if special care is taken on the sample positioning on the weighing table and cleanliness during sample handling and preparation. The magnification in Fig. 7(b) shows results for samples coated with area densities lower than 0.2 g/m^2. This results lead to the conclusion that the limit of detection of the calibrated laser scanner is better than 0.05 g/m^2 for the lubricant KTL N 16.

Optics EXPRESS

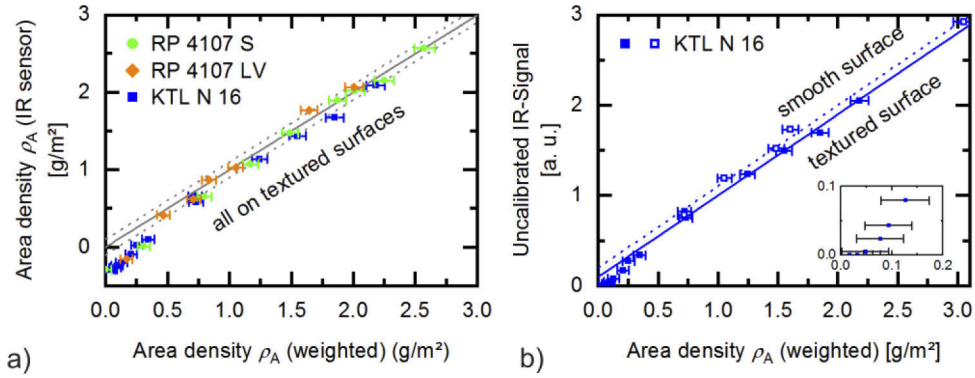

Fig. 8. Characterization of the IR sensor. The plots show the results for three different oil types on the same substrate (a) and one oil type applied on two different steel substrates (b). For this analysis, the lubricant layers were gravimetrically characterized using a high-resolution balance as reference. The continuous gray line in the left plot (a) indicates the ideal correlation between the balance and the IR sensor. The dashed gray lines indicate a deviation of ± 0.1 g/m^2.

All in all, the presented results prove that the analysis of gravimetrically characterized samples provide a convenient way for the calibration of lubricant layers larger than 0.2 g/m^2. The strongest drawback of this method is that these calibrations have to be repeated for each combination of analysis system, functional coating as well as substrate material individually.

4.2. Calibration method 2: infrared absorption measurements as reference

The characterization of this calibration method is split into two sections. In a first step, the characteristics of the IR sensor is analyzed. In a second step, we analyze a possible usage of the IR sensor for the calibration of the fluorescence sensor.

The plots in Fig. 8 show the results for the characterization of the NG 2 IR sensor. Each diagram compares the measurement results of the IR sensor with the gravimetric characterization of the samples using the high-resolution balance. For this experiment, we used the same samples as for the characterization of calibration method 1.

Figure 8(a) shows the analysis of EDT textured steel samples coated with three different lubricants. For the acquisition of the results shown in Fig. 8(a), calibration data for the appropriate steel surface is loaded in the IR sensor. All lubricants were measured with the same calibration data, since they are all mineral oil based and hence have a similar ratio between their molecular weight and their number of C-H bonds. The presented results clearly indicate that the response of the IR sensor is independent of the lubricant type for the oil types used in this work. The average deviations between the area densities measured with the IR sensor and the area densities determined with the high resolution balance are $\Delta\rho_{A,Ø} = \pm 0.12$ g/m^2 for KTL N 16, $\Delta\rho_{A,Ø} = \pm 0.06$ g/m^2 for RP 4107 LV, and $\Delta\rho_{A,Ø} = \pm 0.06$ g/m^2 for RP 4107 S in the range from 0.5 to 2.5 g/m^2. For lubricant coatings less than 0.5 g/m^2, the calibration data used in this experiment is not valid. The magnification in Fig. 8(b) shows the uncalibrated sensor response for layers of KTL N 16 on EDT textured steel that are thinner than 0.25 g/m^2. As indicated in this magnification, the limit of detection of the IR sensor used in this work is better than 0.1 g/m^2.

Figure 8(b) compares the uncalibrated response of the IR sensor for layers of the forming oil KTL N 16 applied on an EDT textured steel surface as well as on a smooth aluminum silicate coated steel surface. The results show a slightly dependency of the signal offset as function of the substrates' surface properties.

Optics EXPRESS

Overall, the sensor response of the IR sensor is significantly less dependent on the lubricant type and the surface properties compared to the results of the fluorescence measurements of the same samples presented in Fig. 7.

As discussed before, we used the measurement results of the IR sensor for the calibration of the fluorescence laser scanner. Figure 9 shows the correlation between the results of both sensors for lubricant layers in the range from 0.5 to 3 g/m^2.

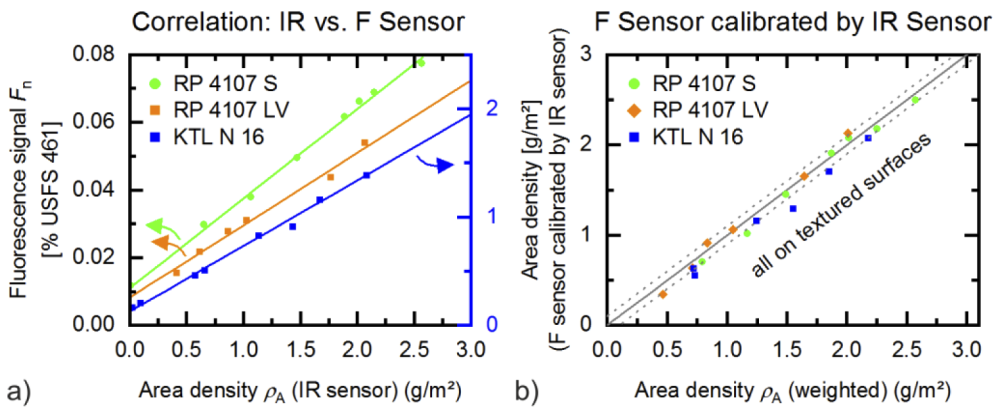

Fig. 9. Calibration of the fluorescence laser scanner (F sensor) for three different oil types applied on EDT textured steel. As reference method, the lubricant layers are characterized using the calibrated infrared absorption sensor (IR sensor). The left plot (a) shows the correlation between both sensor signals. The right plot compares the area densities determined with the calibrated F sensor to the area densities determined using the high precision balance. The dashed gray lines indicate a deviation of ± 0.1 g/m^2.

The results in Fig. 9(a) clearly visualize a linear relation between the detected fluorescence signals and the area density of lubricant optically determined with the calibrated infrared absorption sensor. All lubricants and surface materials analyzed in this work show a linear relation between the sensor responses of both systems. The linear calibration functions describing the relation between both sensors are plotted as continuous lines in Fig. 9(a). The average deviations between the linear fit function and the sample measurements are $\Delta\rho_{A,Ø} = \pm 0.04$ g/m^2 for KTL N 16, $\Delta\rho_{A,Ø} = \pm 0.06$ g/m^2 for RP 4107 LV, and $\Delta\rho_{A,Ø} = \pm 0.04$ g/m^2 for RP 4107 S applied on EDT textured steel surfaces. The average relative deviation between the linear fit function and the sample measurements for all samples is $\Delta\rho_{A,Ø} = \pm 4\%$.

To determine the accuracy of this method, we calculate the area density of each sample measured with the fluorescence laser scanner by applying the calibration data gathered from the results presented in Fig. 9(a). The plot in Fig. 9(b) compares this calculated area densities to the area densities determined using the high precision balance. The average deviations between the area densities measured with the IR calibrated fluorescence laser scanner and the area densities determined with the high resolution balance are $\Delta\rho_{A,Ø} = \pm 0.15$ g/m^2 for KTL N 16, $\Delta\rho_{A,Ø} = \pm 0.07$ g/m^2 for RP 4107 LV, and $\Delta\rho_{A,Ø} = \pm 0.08$ g/m^2 for RP 4107 S.

4.3. Calibration method 3: multiphase carbon analyzer measurements as reference

Figure 10 exemplarily shows the result for the calibration of the fluorescence laser scanner for a rolling oil applied on copper samples. After each fluorescence measurement, the amount of coating applied on the samples surface was determined using a previously calibrated multiphase carbon analyzer.

As shown in Fig. 10, the rolling oil used in this experiment emits only weak fluorescence signals compared to the lubricants analyzed with method 1 and 2. Despite this weak emission, the

Optics EXPRESS

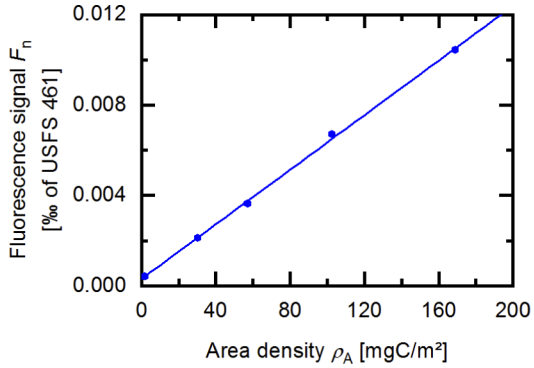

Fig. 10. Calibration of the fluorescence laser scanner for a rolling oil applied on copper sample. As reference method, the lubricant layers are characterized using a calibrated multiphase carbon analyzer. The multiphase carbon analyzer determines the total amount of carbon on the sample surface in milligram carbon per square meter (mgC/m^2). [9]

results show a good linear relation between the normalized fluorescence signal F_n and the total amount of carbon determined by the multiphase carbon analyzer. The continuous line plotted in Fig. 10 visualizes this linear relation. The average deviation between the linear fit function and the sample measurements is $\Delta\rho_{A,Ø} = \pm\, 1.4$ mgC/m^2 or $\Delta\rho_{A,Ø} = \pm 2\%$.

This result clearly shows that a multiphase carbon analyzer can be used to calibrate the developed imaging fluorescence measurement systems. Further work has to be done to determine the relation between the amount of carbon on the surface detected by the multiphase carbon analyzer and the actual area density of the lubricant.

4.4. Calibration method 4: printing of defined lubricant layers

For the characterization of this calibration method, we printed different area densities of the lubricant oil BAM K-009 on a sand blasted aluminum surface. Figure 11(a) shows the fluorescence image of the coated aluminum surface acquired by the fluorescence laser scanner. Figure 11(b) shows the average normalized fluorescence response F_n of each layer as function of the printed area density ρ_A.

The results presented in Fig. 11(b) show good linear relation between the normalized fluorescence signal F_n and the area density printed on the surface. The continuous line plotted in Fig. 11(b) visualizes this linear relation. The average deviation between the linear fit function and the sample measurements is $\Delta\rho_{A,Ø} = \pm\, 6.9$ mg/m^2 or $\Delta\rho_{A,Ø} = \pm 3\%$.

In practice, it has to be considered that time-consuming trials have to be done for the determination of appropriate settings of the ink-jet printer. In addition, it has to be considered that based on the sample surface properties the printed oil droplets behave differently. The contact angles of the droplets and the distance between droplets determine whether the single droplets merge to a closed homogeneous lubricant layer.

4.5. Calibration method 5: Use of thin film cuvettes and device independent transfer of spectrometer measurements using a reference target

Figure 12(a) shows the fluorescence spectra acquired with the fluorescence spectrometer. The plot shows the result for three samples excited with light at 405 nm wavelength: a cuvette filled with a 37 µm thick layer of the forming oil KTL N 16, a cuvette filled with a 260 µm thick layer of lubricant for corrosion protection RP 4107 S, and the transfer target USFS 461. Since the transfer target shows a strong fluorescence emission, for this experiment an OD1 neutral density filter was placed in front of the excitation and detection aperture of the spectrometer. Each filter allows

Optics EXPRESS

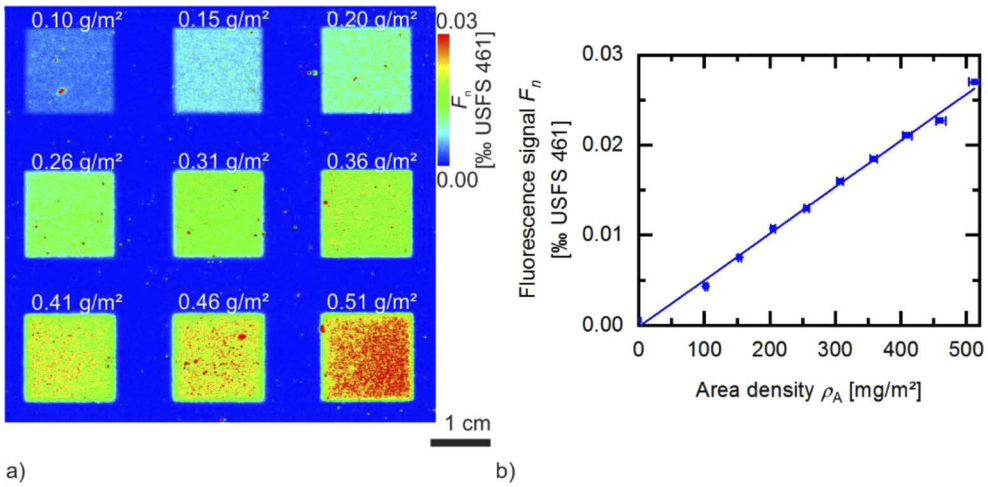

Fig. 11. Calibration of the fluorescence laser scanner for the lubricant oil BAM K-009 applied on sand blasted aluminum surface. The number of oil droplets printed on the surface determines the area density of each lubricant layer. The right diagram (b) shows the evaluation of the fluorescence image of the printed layers shown on the left (a).

a transmission of 10% of light in the spectral range from 400 to 700 nm. Therefore, the use of both filters leads to an attenuation of 99% of the fluorescence emission of the transfer target.

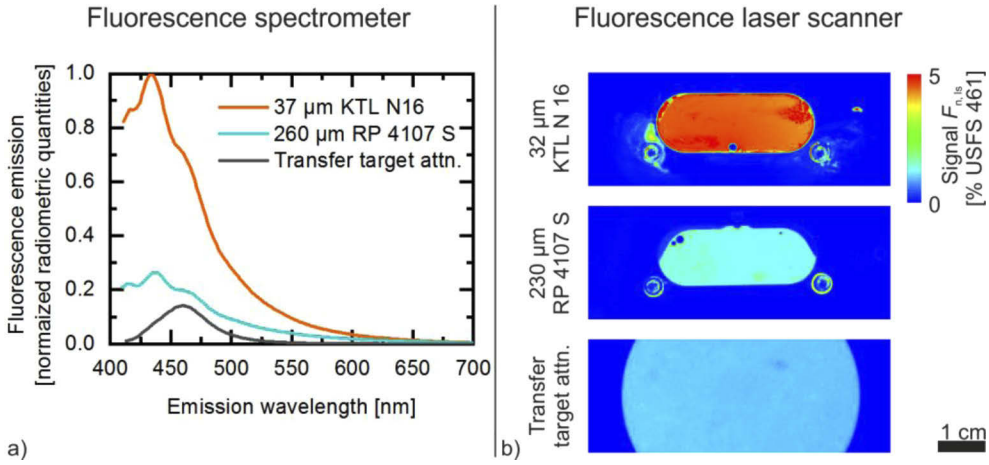

Fig. 12. Fluorescence signals of different cuvettes filled with the lubricants RP 4107 S and KTL N 16 as well as the transfer target USFS 461. The left plot (a) shows the fluorescence spectra F_λ of each sample at excitation with light at 405 nm. The right images (b) show the fluorescence images of both cuvettes as well as the transfer target. To keep all fluorescence intensities in the same order of magnitude, the signal of the transfer target is attenuated using neutral density filters.

Figure 12(b) shows fluorescence images of the same samples. The fluorescence images were acquired with the fluorescence laser scanner directly after the acquisition of the fluorescence spectra. In contrast to the measurements with the spectrometer, one single OD1 filter is placed directly on the surface of the transfer target. Due to the coaxial setup of the laser scanner, both

Optics EXPRESS

the light of the excitation laser and the fluorescence emission pass this single OD1 filter. This again leads to an attenuation of 99% of the fluorescence emission of the transfer target.

As described in the methods section, both the angle of illumination and the angle of the observation of the samples vary between the two fluorescence measurement systems compared in this publication. Therefore, the angular dependency of the fluorescence signal emitted by a liquid filled cuvette as well as the transfer target has to be considered for the transfer of the calibration data between both systems. Figure 13(a) shows the fluorescence signal as function of the viewing angle at orthogonal illumination of both sample types. The results shown in Fig. 13(a) were gathered using the setup presented in Fig. 6(a).

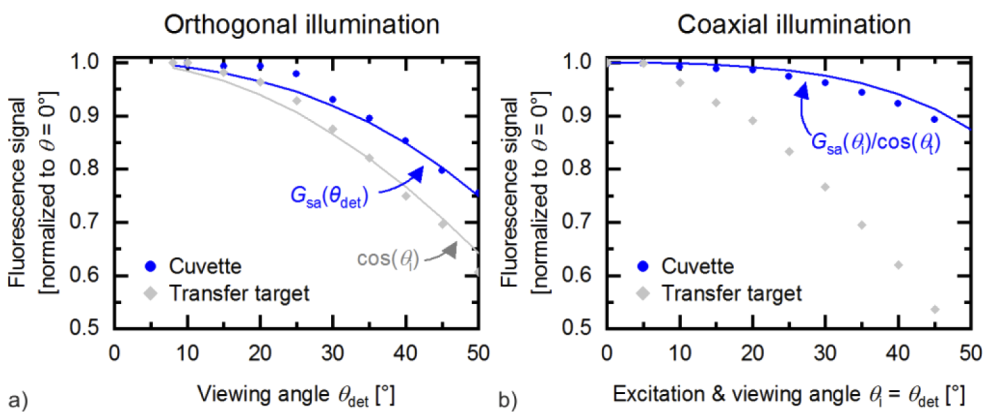

Fig. 13. Angle dependency of the fluorescence signal emitted by a liquid filled cuvette as well as the transfer target USFS 461. The left plot (a) shows the signal as function of the viewing angle at orthogonal illumination of the samples. The experimental setup used to gather this results is visualized in Fig. 7(a). The right plot (b) shows the signal as function of the viewing angle while the sample is illuminated at the same angle as the viewing angle. The experimental setup used to gather this results is visualized in Fig. 7(b).

According to Lambert's cosine law, the radiant intensity emitted by an ideal diffuse radiator is directly proportional to the cosine of the viewing angle θ_{det} between the direction of the emitted light and the surface normal. The projected area that is imaged by a detector with fixed aperture is inverse proportional to the cosine of the viewing angle θ_{det}. Therefore, in general the detected radiance of a Lambertian emitter is independent of the viewing angle. As shown in Fig. 6, the area illuminated by the excitation laser in our setup is smaller than the field of view of the detector optics. In this specific case, the increasing area monitored of the detector with increasing viewing angle θ_{det} does not compensate the decrease of the decreasing radiant intensity with increasing viewing angle. Thus, in our setup the detected radiance of a Lambertian fluorescence emitter decreases directly proportional to the cosine of the viewing angle θ_{det}. The results in Fig. 13(a) visualize the Lambertian emission characteristics of the transfer target used in this work.

The results in Fig. 13(a) show that the angular emission characteristics G_{sa} (θ_{det}) of the filled cuvette is slightly broader in comparison to the characteristics of a Lambertian emitter.

Figure 13(b) presents the detected fluorescence signal as function of the viewing angle while coaxially illuminating the sample at the same angle as the viewing angle. The results shown in Fig. 13(b) were acquired using the setup presented in Fig. 6(b). Compared to the results shown in Fig. 13(a), a stronger signal decrease as function of the viewing angle is monitored for the reference target. In contrast, a lower signal decrease as function of the viewing angle is monitored for the cuvette filled with fluorescent lubricant. This reduced decrease can be explained by the increasing absorption length l of the excitation light according to Eq. (7).

Optics EXPRESS

To sum up, the results in Fig. 13(b) clearly indicate a strong difference in the angular fluorescence characteristics of the transfer target and the cuvette. At an angel of $\theta = 45°$ the signal of the reference target decreases to 54% compared to the signal detected at $\theta = 0°$. In contrast, the signal of the filled cuvette decreases only to 90% at the same tilt of the sample. As described by Eqs. (22) and (23), this effect has to be considered for the transfer of calibration data between the laser scanner and the spectrometer. Using these results, the correction factor C_θ can be determined experimentally from the ratio of the signal decrease applicant in both optical setups. In our case, this leads to a correction factor of $C_\theta = \frac{0.54}{0.9} = 0.61$.

The diagrams presented in Fig. 14 show the normalized fluorescence response F_n of two differently thick cuvettes filled with different lubricants. Each diagram compares the normalized fluorescence response $F_{\mathrm{n,\,sp}}$ acquired with the spectrometer with the normalized response $F_{\mathrm{n,\,ls}}$ detected with the laser scanner. The normalized fluorescence response $F_{\mathrm{n,\,sp}}$ of the spectrometer plotted in Fig. 14(a) is calculated by the integration of the complete fluorescence spectra F_λ shown in Fig. 12(a). The normalized fluorescence response $F_{\mathrm{n,\,ls}}$ of the laser scanner is calculated by analyzing the average detector signal of the fluorescence images of the samples shown in Fig. 12(b). The results in Fig. 14(a) show a deviation between this raw data acquired with both optical setups of over 100%. As described in Eqs. (19) and (22), the raw data of the spectrometer measurements has to be adjusted to the spectral properties of the laser scanner. Therefore, only the spectral emission in the wavelength range from $\lambda_\mathrm{l} = 420$ to $\lambda_\mathrm{h} = 500$ nm has to be considered. Figure 14(b) shows the results considering this spectral correction C_s. These spectrally corrected results still show a deviation of over 90%. Figure 14(c) shows the results after the additional application of the correction C_θ of the angular emission properties.

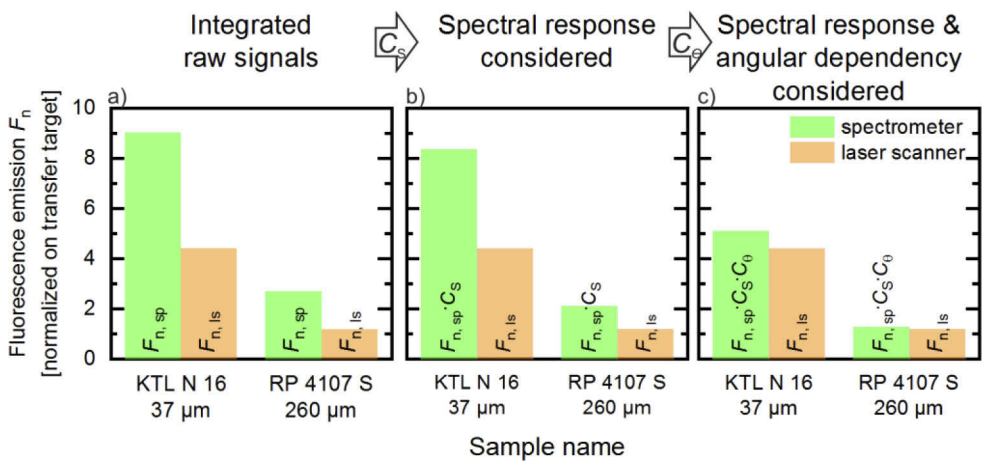

Fig. 14. Fluorescence signals of different cuvettes filled with the lubricants RP 4107S and KTL N 16. Each plot compares the signals acquired with a fluorescence spectrometer with the signals acquired with an imaging fluorescence laser scanner. All fluorescence signals are normalized on the signal of the fluorescent transfer target USFS 461. Simple analysis of the raw signals (a) as well as considering the correction factor C_S describing the spectral response of both systems (b) lead to different results for both systems. For comparable results, the correction C_θ describing the angular dependency of the fluorescence emission has to be considered additionally (Fig c).

As shown in Fig. 14(c), the spectral and angular corrections described in Eq. (22) lead to a reduction of the deviation to better than 15%. For the acquisition of the fluorescence spectra, the positioning of the sample is crucial to the signal amplitude detected. While the custom-made cuvette has a rectangular shape, the transfer target used in this work is realized as a two inch

Optics EXPRESS

disc. The remaining deviation can possibly be explained with slightly different positions of both samples inside the sample chamber of the spectrometer due to their different geometrical shapes. A further probable reason for the remaining deviation of 15% is the simplified assumption of identical angles $\theta_i = \theta_{det} = 45°$ for both illumination as well as observation for the fluorescence spectrometer. According to the Fresnel equations, different angles of incidents lead to a variation of the reflectance at the interface between media with different refractive indices [13]. This leads to a variation of the portion of the excitation light reflected at the interface between air and sample. As the spectrometer uses non-polarized light for the fluorescence excitation, this effect can be neglected.

To sum up, the presented method allows the transfer of calibration data between fluorescence measurement systems with different optical setups. However, the results indicate that the error induced by this method increases with the degree of difference between the optical setups.

It is commonly known that for the reason of quality assurance instrument performance has to be regularly validated at fixed application-relevant measurement conditions to, e.g., detect changes of the optical and optoelectronic components of the instrument [16]. The transfer target used for this method can be used for this instrument performance validation.

5. Conclusion and outlook

We have implemented and characterized five different methods for the calibration of fluorescence sensors. To evaluate the precision of the different calibration methods, we determined the mean deviation of the samples used for calibration from the linear calibration function. Table 2 summarizes the results for the different calibration methods. It has to be considered that different lubricant types have been used for the characterization of the different calibration methods.

Table 2. Comparison of the precision of the presented calibration methods. The table shows the mean deviation of the samples used for calibration from the linear calibration function.

Calibration by	Recommended sample range	Mean deviation $\Delta\rho_{A,\varnothing}$
High precision balance	$\rho_A > 0.2$ g/m^2	±50 mg/m^2
Infrared absorption sensor	$\rho_A > 0.2$ g/m^2	±50 mg/m^2
Multiphase carbon analyzer	$\rho_A < 0.2$ g/m^2	±1 mgC/m^2
Printing of lubricant layers	$\rho_A < 0.5$ g/m^2	±7 mg/m^2

The use of a multiphase carbon analyzer as well as the printing of thin lubricant layers lead to the lowest absolute scattering of the calibration values. Therefore, these methods can be used to determine the limit of detection of fluorescence sensors in lab environments.

For fluorescent layers down to 0.2 g/m^2, a high precision balance can be used as reference for calibration. The main advantages of this method are the comparably easy sample preparation and direct traceability. Nevertheless, this calibration method requires a clean and vibration free lab environment, too.

We suggest two possibilities to overcome the requirement of a lab environment for calibration. As first possibility, we presented the use of a previously calibrated infrared absorption sensor for the calibration of fluorescence sensors. The results presented in this paper show a mean deviation of only $\Delta\rho_{A,\varnothing} = \pm 0.1$ g/m^2 between the area densities measured with the IR calibrated fluorescence laser scanner and the area densities directly determined with a high- resolution balance. We characterized both sensor types separately to determine their limit of detection and parameters influencing their signal response. In contrast to the fluorescence sensor, the results of the IR absorption sensor are significantly less dependent on both lubricant and surface material for the lubricants analyzed in this paper. On the other hand, the drawback of the suggested IR sensor technology is a low sampling rate, which does not allow imaging measurements of thin layers at typical production speeds. Therefore, the combination of both measurement technologies allows

Optics EXPRESS

a robust quantitative and spatially resolved inline measurement of e.g. lubricant layer on metal sheets. Figure 15 visualizes a concept for an auto calibrating inline fluorescence measurement system for the analysis of lubricant layers on moving metal strips.

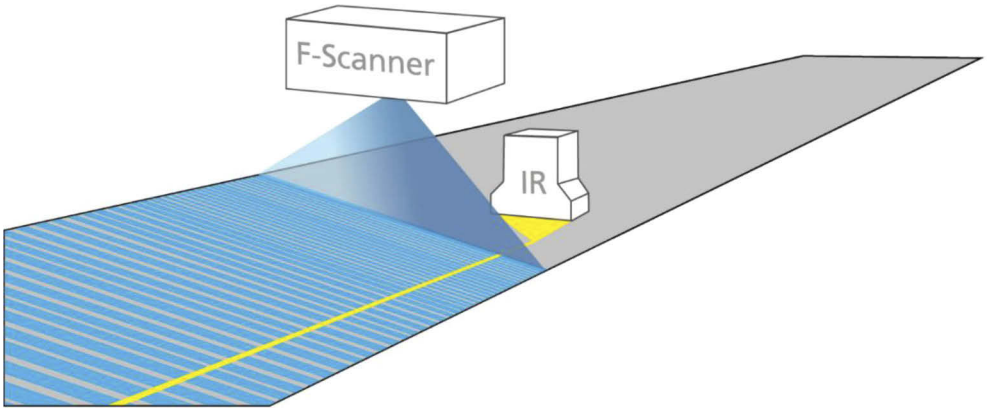

Fig. 15. Auto calibration of an imaging fluorescence laser scanner (F-Scanner) by a single point IR sensor (IR). The suggested concept combines the advantages of both measurement technologies. Fluorescence measurement systems allow high sampling rates and therefore allow imaging inline measurements. Infrared measurement systems are less dependent on layer and substrate properties compared to fluorescence sensors.

Further work is required for the implementation and characterization of the combined sensor concept directly in industrial environments.

As second possibility to overcome the requirement of a clean lab environment, this work for the first time shows the transfer of calibration data between different optical setups by using a solid material fluorescence standard as transfer target. The presented results show an error of less than 15% for the transfer of calibration data acquired with a fluorescence spectrometer onto a fluorescence laser scanner. Improvements are expected for more similar optical setups. Further work can be done to investigate the optimal transfer target for the developed method. For example, dye doped polymer layers or glasses doped with rare-earth-ions could be used as transfer targets [23,24].

Funding

Bundesministerium für Wirtschaft und Energie (ZF4036504 PO6).

Acknowledgment

We thank Mr. Huth-Fehre from Infralytic GmbH for both the teamwork in the lab during the measurements with the IR sensor as well as the fruitful discussions regarding the combination of both sensor types.The work presented in this publication was done in the group Optical Surface Analytics at Fraunhofer IPM. We thank Christoph Pönisch for the pilot tests leading to the experiments for the transfer of calibration results presented in this publication. We thank Laura Engel for supporting us with printing the lubricant layers.

References

1. A. M. Lefcourt, M. Wiederoder, N. Liu, M. S. Kim, Y. M. Lo, K. Chao, N. Liu, M. S. Kim, Y. M. Lo, and K. Chao, "Portable hyperspectral imaging system for monitoring the efficacy of sanitation procedures in produce processing plants," in *Proceedings of 3rd Workshop on Hyperspectral Image and Signal Processing: Evolution in Remote Sensing* (IEEE, 2011), pp. 1–4.

Optics EXPRESS

2. T. Hengstermann and R. Reuter, "Lidar fluorosensing of mineral oil spills on the sea surface," Appl. Opt. **29**(22), 3218–3227 (1990).
3. S. Wigger, H.-J. Füßer, D. Fuhrmann, C. Schulz, and S. A. Kaiser, "Quantitative two-dimensional measurement of oil-film thickness by laser-induced fluorescence in a piston-ring model experiment," Appl. Opt. **55**(2), 269 (2016).
4. P. Holz, C. Lutz, and A. Brandenburg, "Optical scanner system for high resolution measurement of lubricant distributions on metal strips based on laser induced fluorescence," Proc. SPIE **10329**, 103292A (2017).
5. U. Resch-Genger and P. C. DeRose, "Fluorescence standards: Classification, terminology, and recommendations on their selection, use, and production (IUPAC Technical Report)," Pure Appl. Chem. **82**(12), 2315–2335 (2010).
6. C. H. Hidrovo and D. P. Hart, "Emission reabsorption laser induced fluorescence (ERLIF) film thickness measurement," Meas. Sci. Technol. **12**(4), 467–477 (2001).
7. A. C. Jones, M. Millington, J. Muhl, J. M. De Freitas, J. S. Barton, and G. Gregory, "Calibration of an optical fluorescence method for film thickness measurement," Meas. Sci. Technol. **12**(5), N23–N27 (2001).
8. A. Earp, C. E. Hanson, P. J. Ralph, V. E. Brando, S. Allen, M. Baird, L. Clementson, P. Daniel, A. G. Dekker, P. R. C. S. Fearns, J. Parslow, P. G. Strutton, P. A. Thompson, M. Underwood, S. Weeks, and M. A. Doblin, "Review of fluorescent standards for calibration of in situ fluorometers: Recommendations applied in coastal and ocean observing programs," Opt. Express **19**(27), 26768 (2011).
9. P. Holz and A. Brandenburg, "Fluorescence laser scanner for in-line inspection of functional coatings in metal processing industries," Proc. SPIE **11056**, 110561X (2019).
10. J. R. Lakowicz, *Principles of Fluorescence Spectroscopy* (Springer, US, 2006).
11. C. Würth, M. Grabolle, J. Pauli, M. Spieles, and U. Resch-genger, "Relative and absolute determination of fluorescence quantum yields of transparent samples," Nat. Protoc. **8**(8), 1535–1550 (2013).
12. U. Resch-Genger, *Standardization and Quality Assurance in Fluorescence Measurements II* (Springer, Verlag Berlin Heidelberg, 2008)
13. E. Hecht, *Optik, 5th ed.* (Oldenbourg, Verlag, 2009).
14. B. Valeur, *Molecular Fluorescence* (Wiley, VCH Verlag GmbH, 2001), 8.
15. C. Monte, U. Resch-Genger, D. Pfeifer, D. R. Taubert, and J. Hollandt, "Linking fluorescence measurements to radiometric units," Metrologia **43**(2), S89–S93 (2006).
16. U. Resch-Genger, *Standardization and Quality Assurance in Fluorescence Measurements I* (Springer, Verlag Berlin Heidelberg, 2008)
17. Labsphere Inc., "Datasheet Spectralon Diffuse Fluorescence Materials," http://labsphere.com/labsphere-products-solutions/materials-coatings-2/coatings-materials/fluorescence-materials/.
18. P. Doraciak, A. Bünting, and T. Lampke, "Surface inspection of joint areas by means of laser-induced breakdown spectroscopy," IOP Conf. Ser.: Mater. Sci. Eng. **480**(1), 012006 (2019).
19. Y. Luzinova, B. Zdyrko, I. Luzinov, and B. Mizaikoff, "Detecting trace amounts of water in hydrocarbon matrices with infrared fiberoptic evanescent field sensors," Analyst **137**(2), 333–341 (2012).
20. M. T. Romero and N. Ferrer, "Determination of oil and grease by solid phase extraction and infrared spectroscopy," Anal. Chim. Acta **395**(1-2), 77–84 (1999).
21. Leco Corporation, "Application Note: Surface Carbon on Steel Sheet and Rod Samples," (2008).
22. U. Panne and I. Nehls, "Datasheet: Certified Reference Material BAM-K009," https://rrr.bam.de/RRR/Content/EN/Downloads/RM-Certificates/RM-cert-environment/bam_k009.html.
23. C. Brunner, K. Hoffmann, T. Thiele, U. Schedler, H. Jehle, and U. Resch-Genger, "Novel calibration tools and validation concepts for microarray-based platforms used in molecular diagnostics and food safety control," Anal. Bioanal. Chem. **407**(11), 3181–3191 (2015).
24. K. Hoffmann, M. Spieles, W. Bremser, and U. Resch-Genger, "Narrow-Band Emitting Solid Fluorescence Reference Standard with Certified Intensity Pattern," Anal. Chem. **87**(14), 7204–7210 (2015).